J CLIN PRACT RES

Original Article

Official Journal of Erciyes University Faculty of Medicine

DOI: 10.14744/cpr.2026.70711
J Clin Pract Res 2026;48(4):411–421

Multi-Omics Integration Identifies Ferroptosis-Related miRNA–mRNA Networks and Independent Prognostic miRNAs in Triple-Negative Breast Cancer

Selim Öğüt,[1] Ebru Cingöz Çapan,[2] Günnaz Çapan,[3] Serap Yeşilkır Baydar,[4] Abbas Ali Husseini[4]

[1]Department of Basic Medical Sciences, Department of Biophysics, Bandırma Onyedi Eylül University, Faculty of Medicine, Balıkesir, Türkiye
[2]Department of Medical Services and Techniques, Medical Laboratory Techniques Program, Vocational School of Health Services, Avrasya University, Trabzon, Türkiye
[3]Department of Biophysics, Health Sciences Institute, Faculty of Medicine, İstanbul University, İstanbul, Türkiye
[4]Life Sciences and Biomedical Engineering Application and Research Centre, İstanbul Gelişim University, İstanbul, Türkiye

Cite this article as:
Öğüt S, Cingöz Çapan E, Çapan G, Yeşilkır Baydar S, Husseini AA. Multi-Omics Integration Identifies Ferroptosis-Related miRNA–mRNA Networks and Independent Prognostic miRNAs in Triple-Negative Breast Cancer. JClinPractRes2026;48(4):411–421.

Address for correspondence:
Abbas Ali Husseini.
Life Sciences and Biomedical Engineering Application and Research Centre, İstanbul Gelişim University, İstanbul, Türkiye
Phone: +90 544 388 45 11
E-mail:
husseini.hazara@gmail.com

Submitted: 22.01.2026
Revised: 22.06.2026
Accepted: 25.06.2026
Available Online: 17.08.2026

Erciyes University Faculty of Medicine Publications - Available online at www.jcpres.com

ABSTRACT

Objective: This study aimed to comprehensively characterize the transcriptomic and proteomic landscape of ferroptosis-associated mRNAs, miRNAs, and proteins, elucidate subtype-specific regulatory networks, and identify potential prognostic biomarkers in triple-negative breast cancer (TNBC).

Materials and Methods: Using the TCGA-BRCA cohort for discovery and the METABRIC dataset for validation, we performed differential expression and functional enrichment analyses comparing TNBC and non-TNBC subtypes. An integrated miRNA–mRNA regulatory network was constructed, and multivariable Cox proportional hazards regression analysis was performed to evaluate the prognostic value of the identified biomarkers.

Results: TNBC exhibited profound transcriptional dysregulation, characterized by the marked upregulation of the iron-sequestering gene FTMT ($log_2FC=5.60$) and downregulation of the iron exporter SLC40A1 ($log_2FC=-3.13$). We identified 197 significantly dysregulated miRNAs, including the overexpressed oncomiR hsa-miR-135b and the suppressed tumor-suppressor miRNA hsa-miR-449a. Functional enrichment analyses consistently highlighted substantial disruptions in iron homeostasis and oxidative stress pathways. Network analysis identified NQO1 and SLC38A1 as central mRNA hubs. Notably, although specific mRNAs, including SLC40A1 and ALOX15, demonstrated prognostic value in univariate analyses, multivariable Cox regression analysis revealed that only hsa-miR-378c and hsa-miR-449a remained significant as independent prognostic factors.

Conclusion: This multi-omics integration maps the ferroptosis-related regulatory landscape of TNBC. Although specific mRNAs serve as key structural hubs, hsa-miR-378c and hsa-miR-449a emerge as robust independent prognostic biomarkers, providing important insights into TNBC risk stratification and potential targeted therapeutic strategies.

Keywords: Biomarker, breast cancer, ferroptosis, miRNA, transcriptomic analysis.

INTRODUCTION

Triple-negative breast cancer (TNBC) has received particular attention as an aggressive and treatment-resistant subtype of breast cancer.[1,2] Approximately 40% of patients with TNBC face a high risk of early recurrence and metastatic progression, contributing to poor clinical outcomes.[3] In recent years, ferroptosis, an iron-dependent form of regulated cell death distinct from apoptosis and necrosis, has emerged as a promising therapeutic target in cancer biology because of its potential to eliminate treatment-resistant malignancies by exploiting the metabolic vulnerabilities of cancer cells.[4–7]

MicroRNAs (miRNAs) play a pivotal role in post-transcriptional gene regulation and profoundly affect cancer initiation, progression, and therapeutic response.[8,9] By targeting ferroptosis-related genes, miRNAs can critically modulate ferroptotic processes, underscoring their potential value as biomarkers and therapeutic targets.[10,11] Furthermore, elucidating miRNA-regulated ferroptosis pathways may provide new insights into the molecular pathogenesis of TNBC and facilitate the development of personalized treatment strategies.

However, despite the growing recognition of the role of ferroptosis in cancer, the current literature provides limited data on subtype-specific expression patterns and the prognostic value of ferroptosis-related genes and their regulatory miRNAs in breast cancer. Comprehensive molecular analyses of ferroptosis pathways are therefore essential, particularly in TNBC, to identify novel biomarkers and therapeutic targets. In addition, mapping the interaction networks between ferroptosis-related genes and their regulatory miRNAs is critical for understanding disease mechanisms and developing targeted therapeutic approaches. To address this gap, this study aimed to characterize ferroptosis-related mRNA and miRNA expression patterns in TNBC, identify key biological pathways associated with iron homeostasis and oxidative stress, and construct a miRNA–mRNA regulatory network to identify central hub genes and regulatory miRNAs. This integrative approach may provide insight into ferroptosis regulation in TNBC and support the identification of potential biomarkers and therapeutic targets.

KEY MESSAGES

- TNBC exhibits a distinct "iron-hoarding" transcriptomic profile characterized by marked FTMT upregulation and SLC40A1 downregulation, which disrupt iron homeostasis and increase cellular vulnerability to ferroptosis.
- Regulatory Hubs: Multi-omics integration identified NQO1 and SLC38A1 as central mRNA hubs within a complex miRNA–mRNA network governing the ferroptosis-related regulatory landscape of triple-negative tumors.
- Although many mRNAs demonstrate prognostic potential in univariate analyses, only hsa-miR-378c and hsa-miR-449a emerged as robust independent prognostic biomarkers, offering improved risk stratification for patients with TNBC.

METHODS

Study Design

This study was designed as an integrative bioinformatics analysis of multiple publicly available transcriptomic and proteomic datasets.

Data Sources and Preprocessing

In this study, TCGA-BRCA served as the primary exploratory cohort. RNA sequencing (mRNA), miRNA sequencing profiles, and corresponding clinical data were retrieved from TCGA through the Genomic Data Commons (GDC), which includes patients enrolled between 2006 and 2013. The cohort initially included 1,087 primary breast tumor samples. Patients were classified into TNBC and non-TNBC groups according to the PAM50 intrinsic subtype, with the basal-like subtype defined as TNBC. After quality control and the exclusion of samples with incomplete clinical or molecular data, the final cohort comprised 192 TNBC and 895 non-TNBC cases.

The METABRIC dataset included patients enrolled between 1977 and 2005, comprising 309 TNBC and 1,455 non-TNBC cases, and served as an independent validation cohort for the mRNA-level findings.

Proteomic profiles from the TCGA reverse-phase protein array (RPPA) dataset, which included samples collected between 2011 and 2015, were incorporated to evaluate the protein-level expression of selected ferroptosis-related genes.

The final sample sizes represented the maximum numbers of cases with complete molecular and clinical data after quality control.

Differential Expression Analysis

Differential expression analysis was performed to identify ferroptosis-related mRNAs, proteins, and regulatory miRNAs that were significantly altered between the TNBC and non-TNBC subtypes. For the transcriptomic data, mRNA-seq and miRNA-seq profiles were analyzed using the DESeq2 package with a negative binomial generalized linear model. Differential expression was defined as a false discovery rate

(FDR)-adjusted p-value (padj)<0.05 and an absolute log2 fold change (|log2FC|)>1. Proteomic data were evaluated using the limma package. Because protein expression has a smaller dynamic range than transcript expression, significant protein alterations were defined as padj<0.05 and |log2FC|>0.5. No additional covariates were included in the primary models because preliminary inspection indicated minimal batch effects. The results were visualized using volcano plots, and differentially expressed molecules were prioritized for downstream functional annotation and network integration.

Functional Enrichment and Pathway Analyses

A comprehensive Gene Ontology (GO) enrichment analysis focusing on biological processes, molecular functions, and cellular components was performed to elucidate the biological roles of the identified ferroptosis-associated miRNAs. Accordingly, the target genes of significant miRNAs were retrieved from the multiMiR database, and gene identifiers were converted from Ensembl IDs to Entrez IDs using the bitr function in the clusterProfiler R package. GO biological process, molecular function, and cellular component analyses were then performed to identify overrepresented biological functions and map the functional architecture and regulatory effects of the miRNA–target interactome across the cellular hierarchy, with enrichment significance defined as p<0.05 after correction for multiple testing.

In parallel, Kyoto Encyclopedia of Genes and Genomes (KEGG) pathway analysis was performed on the same gene sets using clusterProfiler to identify enriched pathways associated with ferroptosis, oxidative stress, glutathione metabolism, and other cancer-related signaling processes.

Construction and Analysis of the miRNA–mRNA Regulatory Network

To ensure the biological accuracy of the regulatory landscape, the transcriptomic data were first standardized. Because miRNA expression was initially retrieved at the precursor miRNA (pre-miRNA) level, the precursors were mapped to their corresponding mature sequences using miRBase version 22 annotations. This mapping was critical because mature miRNA strands, rather than their precursors, mediate interactions with mRNAs. All downstream analyses, including target prediction and binding-site classification, were performed using these biologically active mature sequences (Supplementary Table 1).

The network was constructed using only significantly differentially expressed miRNAs (padj<0.05, |log2FC|>1) and significantly differentially expressed ferroptosis-related genes. Interactions were retrieved from miRDB, TargetScan version 8.0, and miRTarBase using the multiMiR package and were included if they were either experimentally validated in miRTarBase or predicted by both TargetScan version 8.0 and miRDB. This process generated a consolidated interaction matrix that was used to construct a directed network in which edges extended from miRNAs to their target genes.

The resulting network was imported into Cytoscape for visualization and topological analysis, and node-level topological parameters, including degree, betweenness centrality, and closeness centrality, were calculated to identify highly connected nodes within the network. High-degree nodes representing hub miRNAs or genes were prioritized as potential key regulators. To assess their biological relevance, these hub molecules were cross-referenced with the published literature on breast cancer progression and ferroptosis regulation, enabling the identification of candidate biomarkers and potential therapeutic targets.

To validate the regulatory potential of the identified hubs, Spearman correlation analysis was performed to evaluate the relationships between the expression levels of miRNAs and their target mRNAs across the dataset. Finally, detailed molecular binding metrics were retrieved for the most critical interactions. These metrics included target-binding regions, seed-match types, and site-conservation status identified using TargetScan and miRDB. Standard nomenclature, including miRBase accession numbers and strand specifications, was maintained throughout the analysis to ensure the full reproducibility of the regulatory model.

Statistical Analysis and Prognostic Modeling

All computational analyses were conducted in the R programming environment, version 4.3.2, using Bioconductor packages. Differential expression analysis was performed using the DESeq2 package, whereas functional enrichment analyses and network visualizations were generated using clusterProfiler, ggplot2, and Cytoscape.

To evaluate the clinical relevance of the identified molecules, Kaplan–Meier curves and univariate Cox regression analyses were used to compare overall survival between the high- and low-expression groups for both mRNAs and miRNAs. The prognostic value of these biomarkers was further assessed using multivariable Cox proportional hazards models, which estimated hazard ratios (HRs) and 95% confidence intervals (CIs). These models were adjusted for clinically relevant covariates, including age and pathological stage, to determine independent prognostic significance. For all statistical tests, p<0.05 was considered statistically significant.

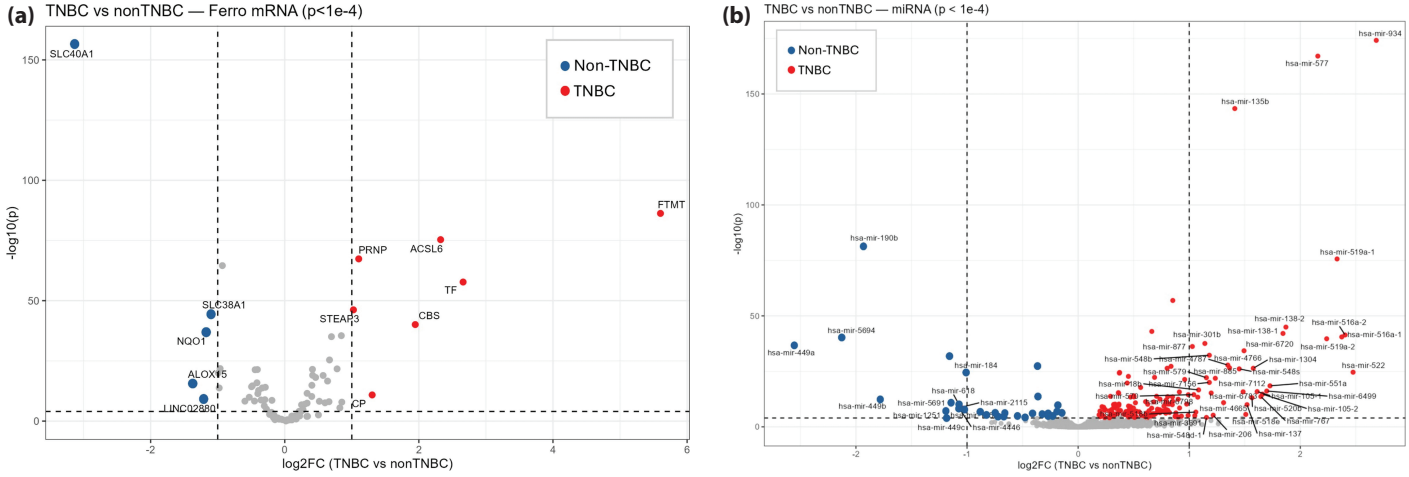

Figure 1. Differential expression of ferroptosis-related mRNAs and miRNAs between TNBC and non-TNBC.

RESULTS

Differential Expression of Ferroptosis-Related Transcripts and Proteins

A curated set of 259 ferroptosis-related genes was compiled from the FerrDb v2 database and recent literature, encompassing known drivers, suppressors, and markers of ferroptotic cell death.[12] Differential gene expression analysis identified several mRNAs with significant expression changes between the TNBC and non-TNBC groups (Fig. 1a). Among the significantly upregulated genes, FTMT ($log_2FC=5.60$, padj<0.001) exhibited the greatest fold increase. Other notably upregulated genes included TF ($log_2FC=2.66$, padj<0.001), ACSL6 ($log_2FC=2.32$, padj<0.001), CBS ($log_2FC=1.95$, padj<0.001), CP ($log_2FC=1.30$, padj<0.001), STEAP3 ($log_2FC=1.02$, padj<0.001), and PRNP ($log_2FC=1.10$, padj<0.001). Conversely, several genes were significantly downregulated, including SLC40A1 ($log_2FC=-3.13$, padj<0.001), SLC38A1 ($log_2FC=-1.11$, padj<0.001), NQO1 ($log_2FC=-1.18$, padj<0.001), ALOX15 ($log_2FC=-1.37$, padj<0.001), and LINC02880 ($log_2FC=-1.20$, padj<0.001).

Differential expression analysis identified 197 miRNAs with statistically significant expression changes between the TNBC and non-TNBC groups (Fig. 1b). A predominantly upregulated pattern was observed, with most significant miRNAs exhibiting positive log_2FC values, suggesting increased miRNA transcriptional activity. Several miRNAs were markedly upregulated. Among these, hsa-miR-135b ($log_2FC=1.41$, padj<0.001), hsa-miR-138-1 ($log_2FC=1.84$, padj<0.001), and hsa-miR-138-2 ($log_2FC=1.87$, padj<0.001) exhibited the most pronounced increases. Other substantially upregulated miRNAs included hsa-miR-130b, hsa-miR-18a, hsa-miR-4766, hsa-miR-188, hsa-miR-3200, hsa-miR-224, and hsa-miR-301b, all of which exhibited padj<0.001 and log_2FC values ranging from 0.32 to 1.36. Conversely, several miRNAs were significantly downregulated. hsa-miR-449a ($log_2FC=-2.56$, padj<0.001) and hsa-miR-190b ($log_2FC=-1.93$, padj<0.001) exhibited the greatest reductions, identifying them as key downregulated regulators. Other markedly downregulated miRNAs included hsa-miR-449b, hsa-miR-449c, hsa-miR-184, hsa-miR-135a-1, hsa-miR-135a-2, and hsa-miR-375 (log_2FC range, -1.78 to -0.60; padj<0.001).

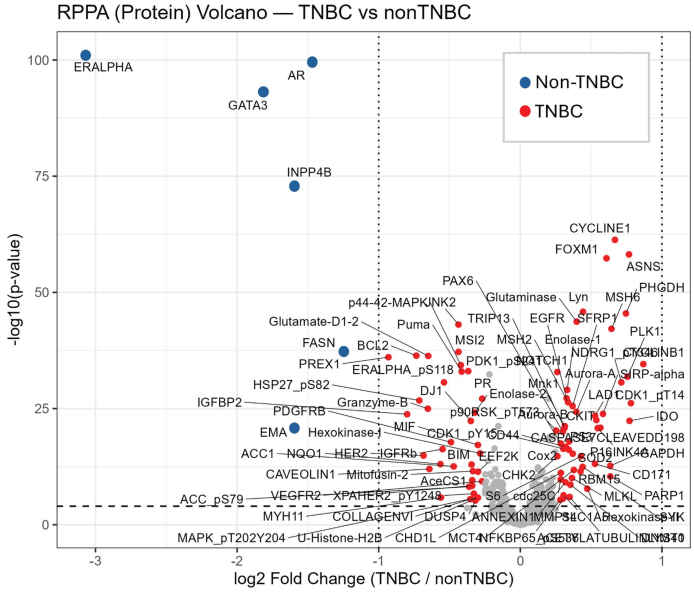

Figure 2. Differential expression of ferroptosis-related proteins between TNBC and non-TNBC.

Reverse-phase protein array analysis of 102 proteins revealed distinct protein expression patterns between TNBC and non-TNBC tumors (Fig. 2). Notably, hormone receptor-related

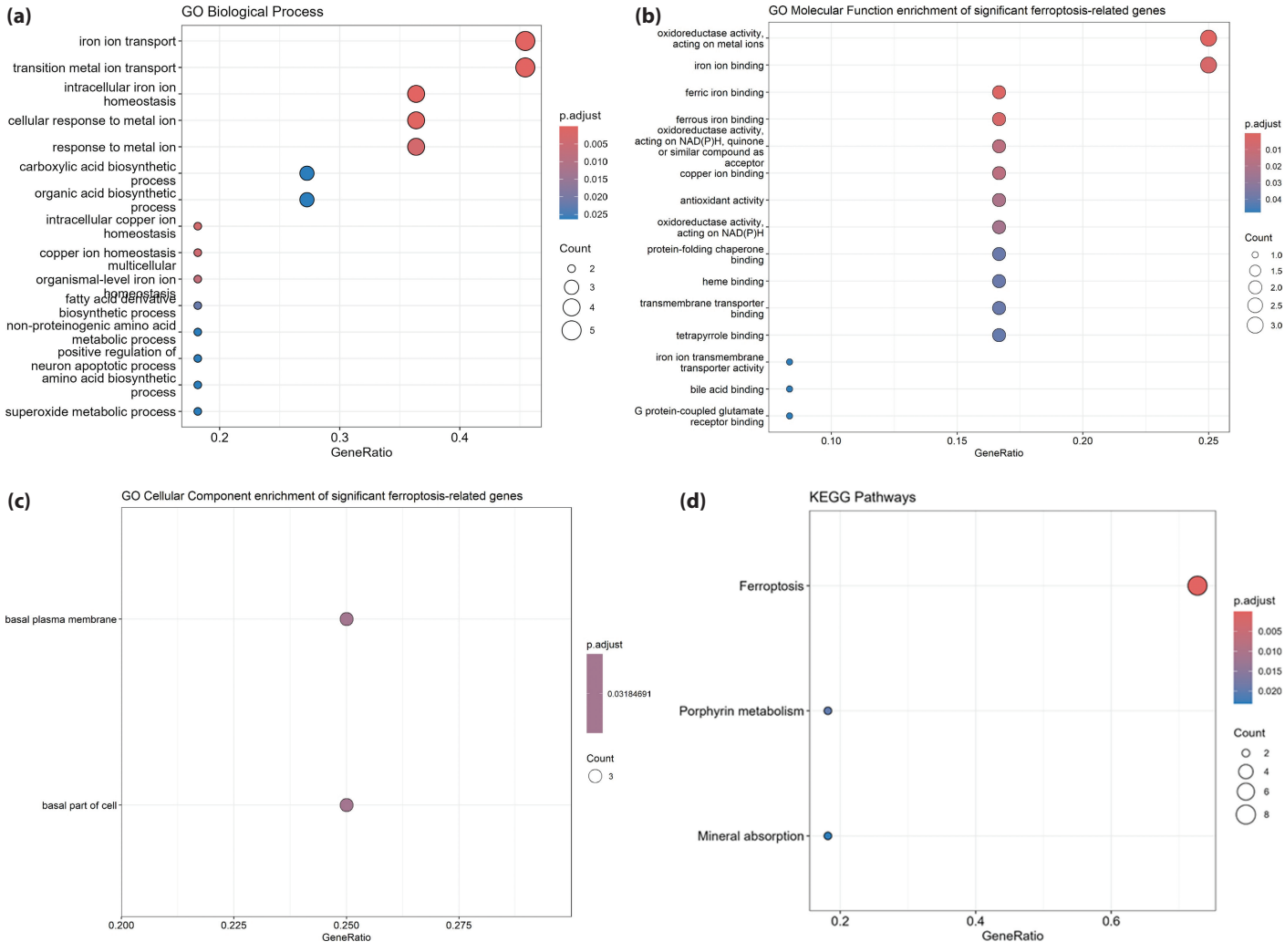

Figure 3. Gene ontology biological process enrichment dot plot for ferroptosis target genes. The y-axis represents the biological processes in which ferroptosis target genes were significantly enriched. The x-axis indicates the GeneRatio, defined as the proportion of analyzed genes associated with a given GO term relative to the total number of genes in that term. Dot size reflects the number of target genes associated with each GO term, whereas color intensity represents the adjusted p-value (padj), with red indicating lower and more statistically significant values.

proteins, including ERALPHA (logFC=-3.07, padj<0.001), AR (logFC=-1.48, padj<0.001), and GATA3 (logFC=-1.82, padj<0.001), were significantly downregulated in TNBC. Conversely, TNBC samples exhibited significant upregulation of proteins associated with cell-cycle regulation, proliferation, and metabolic adaptation. Among these, CYCLIN E1 (logFC=0.67, padj<0.001), ASNS (logFC=0.77, padj<0.001), FOXM1 (logFC=0.61, padj<0.001), PHGDH, MSH6, and CYCLIN B1 were prominently elevated. Altered expression of apoptosis-related proteins, including BCL2, PUMA, and caspase-7, and signaling proteins, such as p44-42-MAPK, PDK1, and IGF1R, further delineated the aggressive phenotype of TNBC.

Transcriptomic Enrichment of Ferroptosis-Related Processes

Functional enrichment analysis revealed a striking convergence of biological processes across both the mRNA and miRNA regulatory layers, primarily centered on iron metabolism and redox homeostasis (Fig. 3a). Gene Ontology analysis of differentially expressed mRNAs showed nominal enrichment in processes including monoatomic cation transport (p=0.044), metal ion transport (p=0.044), and iron ion transport (p=0.045), involving key ferroptosis-related genes such as CP, TF, SLC40A1, and FTMT. Moreover, SLC38A1 was identified as a key participant in glutamine transport;

given that glutaminolysis is a primary driver of ferroptosis, its involvement highlights the metabolic reprogramming that supports ferroptotic vulnerability in TNBC. However, although these transcriptomic changes were subtle and did not remain significant after correction for multiple testing, they were strongly reflected in the regulatory potential of the identified miRNAs. GO enrichment analysis of the target genes regulated by ferroptosis-associated miRNAs revealed an even more robust signature. The most significantly enriched process was iron ion transport (GO:0006826; padj<0.001), involving many of the same core genes identified in the mRNA analysis, including CP, TF, SLC40A1, and FTMT, along with STEAP3. Closely related processes, such as transition metal ion transport (GO:0000041) and intracellular iron ion homeostasis (GO:0006879), were also highly represented, further supporting the involvement of these miRNA targets in metal ion regulation.

Furthermore, both datasets highlighted a coordinated response to oxidative stress and lipid processing. miRNA targets were significantly enriched in the cellular response to metal ions (GO:0071248) and the response to oxidative stress, implicating genes such as ALOX15, PRNP, and NQO1.

Functional Profiling and Pathway Validation of the Ferroptosis-Associated Proteome

GO enrichment analysis of the RPPA dataset revealed a broad spectrum of significantly overrepresented biological processes, with a strong emphasis on cellular stress responses, cell death, and immune regulation. The most significantly enriched terms were related to the intrinsic apoptotic signaling pathway (GO:0097193, padj<0.001), signal transduction in response to DNA damage (GO:0042770, padj<0.001), and their intersection in the DNA damage-induced intrinsic apoptotic pathway (GO:0008630, padj<0.001). The analysis also highlighted a major role for p53-mediated signaling (GO:0072331) and cell-cycle checkpoint control (GO:0000077), underscoring the importance of maintaining genomic integrity. Concurrently, robust enrichment was observed in processes governing immune cell activation and differentiation, particularly those involving T cells (GO:0050863) and lymphocytes, as well as the regulation of cell-cycle phase transitions (GO:1901987). Key regulatory proteins, such as TP53, BCL2, ATM/ATR, and components of the mTOR and EGFR signaling pathways, were recurrently identified as central nodes across these critical processes, suggesting that they are pivotal integrators of apoptotic, DNA damage-related, and proliferative signals within the dataset.

Molecular Function and Cellular Component Analyses of Ferroptosis Regulators

Molecular function (MF) enrichment analysis further elucidated the biochemical activities underlying the ferroptotic landscape of TNBC (Fig. 3b). The most significant enrichment was observed in oxidoreductase activity acting on metal ions and iron ion binding (padj=0.01), specifically involving both ferric and ferrous forms of iron. This finding was complemented by significant enrichment in iron ion transmembrane transporter activity, providing a molecular basis for the systemic alterations in iron metabolism observed in the pathway analysis. Additionally, the identification of antioxidant activity and oxidoreductase activity acting on NAD(P)H (padj=0.03) underscored the disruption of redox-balancing mechanisms. Notably, the enrichment of G protein-coupled glutamate receptor binding (padj=0.04) provided molecular-level support for the involvement of glutaminolysis pathways, as highlighted by the dysregulation of SLC38A1. Furthermore, cellular component (CC) enrichment analysis identified the basal plasma membrane and basal region of the cell (padj=0.03) as the primary sites of dysregulation (Fig. 3c).

KEGG Pathway Enrichment and Functional Mapping of Ferroptosis Signaling

Functional characterization using KEGG pathway analysis revealed a high concentration of differentially expressed genes within the ferroptosis pathway, which emerged as the most statistically significant term (padj<0.001) (Fig. 3d). This enrichment was characterized by an exceptionally high fold enrichment of 163.58, with 8 of the 11 input genes, including CP, TF, and SLC40A1, mapping directly to this cell-death mechanism. Beyond the core ferroptosis machinery, the analysis identified significant enrichment in porphyrin metabolism (padj=0.019) and mineral absorption (padj=0.023).

Construction and Analysis of Regulatory Networks

The constructed miRNA–gene regulatory network revealed a sparse but modular topology, consisting of miRNAs with limited but specific connections to their target genes (Fig. 4). Topological analysis of the miRNA–gene regulatory network, comprising 19 nodes and 15 edges, revealed a hub-driven structure with a network density of 0.0439 and an average degree of 1.58. Network centrality analysis (Supplementary Table 2) indicated that hsa-miR-449a had the highest degree (2) and closeness centrality (0.75) among the miRNAs, suggesting a relatively central regulatory role. In contrast, hsa-miR-618 and hsa-miR-421 exhibited high closeness centrality values (1.0) despite having only one connection, implying direct regulation of highly central genes. Among the target genes, NQO1 and SLC38A1 emerged as hub nodes (degree=4; closeness centrality=0.357), representing major integration points of miRNA regulation. Other genes, such as STEAP3 and ALOX15, showed moderate connectivity, whereas ACSL6 and SLC40A1 exhibited high closeness centrality values (1.0), indicating topological importance despite having few interactions.

Figure 4. Constructed miRNA–gene regulatory network.

Furthermore, Spearman correlation analysis was performed between the expression levels of the miRNAs and their target mRNAs to validate the predicted miRNA–mRNA interactions. Significant negative correlations were observed, supporting the suppressive regulatory relationships of these pairs. Notably, hsa-miR-421 expression was strongly inversely correlated with SLC40A1 expression (Spearman r=-0.279, p<0.001). Other significant negative correlations included those between hsa-miR-378c and SLC38A1 (r=-0.130, p<0.001), hsa-miR-449a and STEAP3 (r=-0.087, p<0.001), hsa-miR-636 and SLC38A1 (r=-0.077, p<0.001), and hsa-miR-618 and ACSL6 (r=-0.070, p=0.023) (Table 1).

Integrated network and Spearman correlation analyses (Table 1) prioritized five key miRNA–mRNA regulatory pairs. For hsa-miR-421-5p and hsa-miR-449a-5p, the correlation-based evidence directly overlapped with the primary TargetScan predictions of SLC40A1 and STEAP3, respectively. However, for hsa-miR-378c and hsa-miR-636, network analysis identified SLC38A1 as the functionally relevant target in the context of TNBC, despite other genes having higher theoretical TargetScan scores (Table 2). All identified interactions were characterized by canonical seed matches within the 3′ untranslated regions of the target mRNAs, providing structural plausibility for the observed expression-based correlations.

mRNA and miRNA Survival and Cox Regression Analyses

Log-rank tests demonstrated significant differences in survival for SLC40A1 (p=0.034) and ALOX15 (p=0.016), whereas FTMT (p=0.46), NQO1 (p=0.67), SLC38A1 (p=0.19), and ACSL6 (p=0.076) did not reach statistical significance (Fig. 5a). In the univariate Cox regression analysis, SLC40A1 (HR=0.71, 95% CI: 0.51–0.98, p=0.035) and ALOX15 (HR=1.49, 95% CI: 1.08–2.07, p=0.017) were significantly associated with overall survival. Conversely, FTMT, NQO1, SLC38A1, and ACSL6 were not significantly associated with survival in the univariate analysis. However, after adjustment for age and pathological stage in the multivariable model, the prognostic significance of SLC40A1 (HR=0.73, 95% CI: 0.49–1.08, p=0.115) and ALOX15 (HR=1.17, 95% CI: 0.77–1.79, p=0.460) was no longer maintained.

Table 1. Spearman correlation analysis of predicted miRNA–mRNA interactions

miRNA	Target gene	Spearman correlation coefficient (r)	p
hsa-miR-421	SLC40A1	-0.279	<0.001
hsa-miR-378c	SLC38A1	-0.130	<0.001
hsa-miR-449a	STEAP3	-0.087	0.004
hsa-miR-636	SLC38A1	-0.077	0.011
hsa-miR-618	ACSL6	-0.070	0.023

The corresponding Kaplan–Meier analysis comparing the low- and high-miRNA-expression groups demonstrated significant differences in survival for hsa-miR-378c (p=0.0001), hsa-miR-449a (p=0.0159), and hsa-miR-3909 (p=0.018). The expression levels of hsa-miR-618 (p=0.101), hsa-miR-7706 (p=0.148), and hsa-miR-1270 (p=0.194) were not significantly associated with survival in the Kaplan–Meier analysis (Fig. 5b). Univariate Cox regression analysis indicated that hsa-miR-378c (HR=1.40, 95% CI: 1.00–1.96, p=0.050) and hsa-miR-449a (HR=0.59, 95% CI: 0.42–0.83, p=0.002) were significant prognostic factors, whereas hsa-miR-3909, hsa-miR-618, hsa-miR-7706, and hsa-miR-1270 were not. In the multivariable Cox regression analysis, both hsa-miR-378c (HR=1.56, 95% CI: 1.03–2.36, p=0.034) and hsa-miR-449a (HR=0.58, 95% CI: 0.38–0.86, p=0.008) remained statistically significant as independent predictors of survival.

DISCUSSION

A central finding of our analysis was the profound dysregulation of iron-handling genes, particularly the marked upregulation of mitochondrial ferritin (FTMT) and suppression of ferroportin (SLC40A1), the sole known cellular iron exporter. This "iron-hoarding" phenotype may, on the one hand, increase intracellular iron levels and promote TNBC progression by providing essential cofactors for enzymes such as ribonucleotide reductase, which directly supports rapid DNA synthesis and tumor cell proliferation.[13,14] On the other hand, iron-dependent reactive oxygen species can activate

Table 2. Molecular characteristics of key predicted miRNA–mRNA interactions

Pre-miRNA (TCGA)	miRBase ID	Network- or correlation-supported target	TargetScan-listed target	Binding region	Seed-match type	Binding site	Prediction/support database	Notes*
hsa-miR-421	MIMAT0003339	SLC40A1	SLC40A1	3′ UTR	7mer-m8	Conserved site	TargetScan, miRDB	
hsa-miR-378c	MIMAT0016847	SLC38A1	PDIA4	3′ UTR	7mer-m8	Conserved site	TargetScan, miRDB	Family-based prediction (miR-378a-3p)
hsa-miR-636	MIMAT0003306	SLC38A1	CETN2	3′ UTR	8mer	Conserved site	TargetScan, miRDB	
hsa-miR-618	MIMAT0003287	ACSL6	LSM1	3′ UTR	7mer-m8	Conserved site	TargetScan, miRDB	
hsa-miR-449a	MIMAT0001541	STEAP3	MDM4	3′ UTR	8mer	Conserved site	TargetScan, miRDB	Predicted through the miR-34 family (representative miRNA: miR-34c-5p)

prosurvival pathways, such as NF-κB and HIF-1α.[15,16] Our results suggest that TNBC exists on a metabolic knife-edge: although iron fuels its aggressive growth, it simultaneously sensitizes tumor cells to lipid peroxidation, thereby creating a targetable vulnerability unique to this subtype.

Our integrative network analysis revealed that this iron-sequestering state is not merely a passive byproduct of cancer but is actively maintained through post-transcriptional regulation. Specifically, the significant inverse correlation between hsa-miR-421 and SLC40A1 suggests that impaired iron export is actively maintained through miRNA-mediated silencing. This regulatory axis identifies hsa-miR-421 as a key driver of the iron-rich phenotype. Furthermore, the identification of hsa-miR-449a as a central regulatory hub is particularly important. Loss of this tumor-suppressor miRNA family may derepress proferroptotic metabolic drivers and oncogenic pathways, further exacerbating the oxidative vulnerability of TNBC cells.[17–20]

Furthermore, we identified SLC38A1, a major glutamine transporter, as a central hub within the regulatory network. Because glutaminolysis is a major driver of ferroptosis, dysregulation of SLC38A1 highlights the metabolic alterations that support ferroptotic vulnerability. This finding was mirrored at the protein level, where TNBC samples exhibited significant upregulation of metabolic adaptation proteins, including PHGDH and ASNS.[21,22] This intersection between nutrient transport and oxidative stress defense demonstrates how the metabolic flexibility of TNBC is structurally supported by its miRNA–mRNA regulatory network.

Although iron-handling genes such as SLC40A1 and ALOX15 demonstrated prognostic significance in univariate analyses, they lost their independent significance after adjustment for clinical covariates, including age and pathological stage. In contrast, hsa-miR-378c and hsa-miR-449a remained independent predictors of survival, suggesting that miRNAs may provide a more integrated and stable representation of tumor behavior than individual mRNA expression levels.

Several limitations should be considered when interpreting our findings. The differential expression analysis was not adjusted for important clinical covariates, which may have introduced confounding effects. In addition, the integration of multiple datasets may have introduced technical batch effects despite normalization procedures. The miRNA–mRNA regulatory networks were primarily based on in silico predictions and correlation analyses without direct experimental validation. Dataset limitations also prevented differentiation between mature miRNA strands (-5p/-3p), resulting predominantly in family-level analyses. Furthermore, the multivariable survival models included only age and tumor stage because of limited clinical annotations. Therefore, our findings should be considered

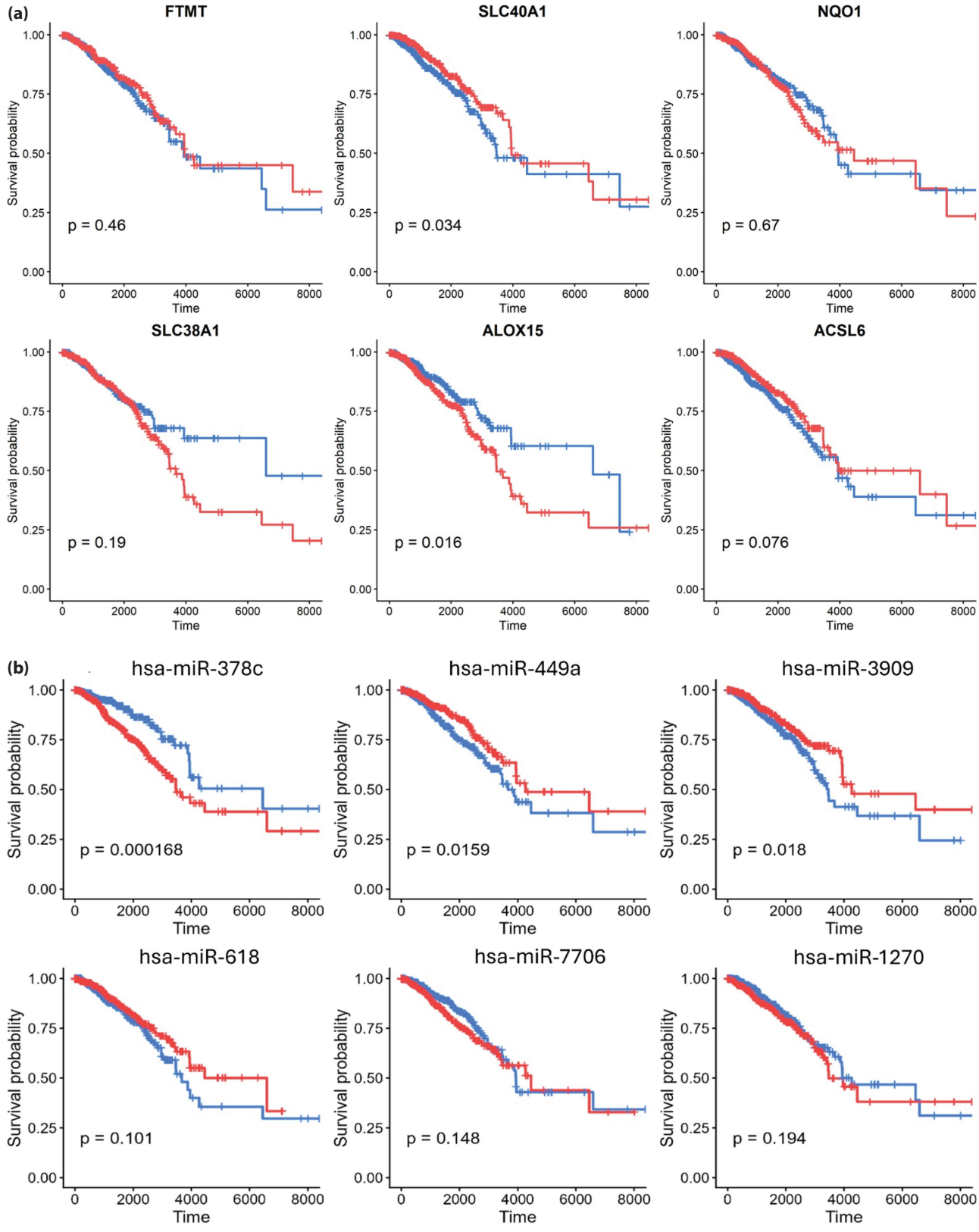

Figure 5. Kaplan–Meier survival curves for hub ferroptosis-related mRNAs and miRNAs in TNBC.

hypothesis-generating and require further in vitro and in vivo validation to confirm their functional relevance in TNBC.

CONCLUSION

This study comprehensively characterized the ferroptosis-related miRNA–mRNA regulatory landscape in TNBC. Although genes such as NQO1, SLC38A1, and SLC40A1 emerged as key regulatory nodes, only hsa-miR-378c and hsa-miR-449a demonstrated independent prognostic value in multivariable survival analyses. These miRNAs may serve as promising biomarkers for risk stratification, whereas the broader mRNA network may provide a framework for developing ferroptosis-targeted therapies in TNBC.

Ethics Committee Approval: Ethics committee approval was not required, as this study was designed as a multi-dataset, integrative bioinformatics analysis using publicly available transcriptomic and proteomic data.

Informed Consent: Written informed consent was not required.

Conflict of Interest: The authors have no conflicts of interest to declare.

Financial Disclosure: The authors declared that this study received no financial support.

Use of AI for Writing Assistance: During manuscript preparation, the authors utilized the OpenAI GPT-4 model to assist with English grammar and spelling corrections. All AI-generated content was reviewed and revised by the authors, who assume full responsibility for the final version of the publication.

Author Contributions: Concept – SÖ, ECÇ, GÇ, AAH; Design – SÖ, ECÇ, GÇ, AAH; Supervision – AAH; Resource – SÖ, AAH; Materials – ECÇ, AAH; Data Collection and/or Processing – SÖ, ECÇ, AAH; Analysis and/or Interpretation – SÖ, ECÇ, SYB, AAH; Literature Review – SYB, AAH; Writing – AAH; Critical Review – AAH.

Peer-review: Externally peer-reviewed.

REFERENCES

1. Lehmann BD, Bauer JA, Chen X, Sanders ME, Chakravarthy AB, Shyr Y, et al. Identification of human triple-negative breast cancer subtypes and preclinical models for selection of targeted therapies. J Clin Invest 2011;121(7):2750-67. [CrossRef]
2. Bianchini G, Balko JM, Mayer IA, Sanders ME, Gianni L. Triple-negative breast cancer: challenges and opportunities of a heterogeneous disease. Nat Rev Clin Oncol 2016;13(11):674-90. [CrossRef]
3. Dent R, Trudeau M, Pritchard KI, Hanna WM, Kahn HK, Sawka CA, et al. Triple-negative breast cancer: clinical features and patterns of recurrence. Clin Cancer Res 2007;13(15 Pt 1):4429-34. [CrossRef]
4. Dixon SJ, Lemberg KM, Lamprecht MR, Skouta R, Zaitsev EM, Gleason CE, et al. Ferroptosis: an iron-dependent form of nonapoptotic cell death. Cell 2012;149(5):1060-72. [CrossRef]
5. Stockwell BR, Friedmann Angeli JP, Bayir H, Bush AI, Conrad M, Dixon SJ, et al. Ferroptosis: A Regulated Cell Death Nexus Linking Metabolism, Redox Biology, and Disease. Cell 2017;171(2):273-85. [CrossRef]
6. Hassannia B, Vandenabeele P, Vanden Berghe T. Targeting Ferroptosis to Iron Out Cancer. Cancer Cell 2019;35(6):830-49. [CrossRef]
7. Jiang X, Stockwell BR, Conrad M. Ferroptosis: mechanisms, biology and role in disease. Nat Rev Mol Cell Biol 2021;22(4):266-82. [CrossRef]
8. Bartel DP. MicroRNAs: genomics, biogenesis, mechanism, and function. Cell 2004;116(2):281-97. [CrossRef]
9. Iorio MV, Croce CM. microRNA involvement in human cancer. Carcinogenesis 2012;33(6):1126-33. Retraction in: Carcinogenesis 2025;47(1):bgaf065. [CrossRef]
10. Blenkiron C, Goldstein LD, Thorne NP, Spiteri I, Chin SF, Dunning MJ, et al. MicroRNA expression profiling of human breast cancer identifies new markers of tumor subtype. Genome Biol 2007;8(10):R214. [CrossRef]
11. Jiang L, Kon N, Li T, Wang SJ, Su T, Hibshoosh H, et al. Ferroptosis as a p53-mediated activity during tumour suppression. Nature 2015;520(7545):57-62. [CrossRef]
12. Zhou N, Bao J. FerrDb: a manually curated resource for regulators and markers of ferroptosis and ferroptosis-disease associations. Database (Oxford) 2020;2020:baaa021. [CrossRef]
13. Gaur K, Pérez Otero SC, Benjamín-Rivera JA, Rodríguez I, Loza-Rosas SA, Vázquez Salgado AM, et al. Iron Chelator Transmetalative Approach to Inhibit Human Ribonucleotide Reductase. JACS Au 2021;1(6):865-78. [CrossRef]
14. Torti SV, Torti FM. Iron and cancer: more ore to be mined. Nat Rev Cancer 2013;13(5):342-55. [CrossRef]
15. Sultana N. Targeting ribonucleotide reductase for breast cancer treatment. Dissertation. University of the Pacific; 2023.
16. Liu L, Bai J, Hu L, Jiang D. Hypoxia-mediated activation of hypoxia-inducible factor-1α in triple-negative breast cancer: A review. Medicine (Baltimore) 2023;102(43):e35493. [CrossRef]
17. Wei KL, Cao XM, Xiong DD, Zeng JJ, Lan AH, Chen G, et al. Downregulation of miRNA-449a expression associated with advanced stages and lymph node metastasis of breast cancer. Int J Clin Exp Pathol 2016;9(7):7370-80.

18. Torres-Ruiz S, Garrido-Cano I, Lameirinhas A, Burgués O, Hernando C, Martínez MT, et al. MiRNA-449 family is epigenetically repressed and sensitizes to doxorubicin through ACSL4 downregulation in triple-negative breast cancer. Cell Death Discov 2024;10(1):372. [CrossRef]
19. Unnikrishnan K, Krishnankutty Chandrika S, Ram Kumar RM, Srinivas P. Tumor Suppressor miRNA-based Signatures in Triple Negative Breast Cancer: A Study Based on Big Data Analysis of Gene Expression Omnibus (GEO) Datasets and Its Validation. Asian Pac J Cancer Prev 2025;26(6):2087-95. [CrossRef]
20. Uva P, Cossu-Rocca P, Loi F, Pira G, Murgia L, Orrù S, et al. miRNA-135b Contributes to Triple Negative Breast Cancer Molecular Heterogeneity: Different Expression Profile in Basal-like Versus non-Basal-like Phenotypes. Int J Med Sci 2018;15(6):536-48. [CrossRef]
21. Mariano NC, Marotti JD, Chen Y, Karakyriakou B, Salgado R, Christensen BC, et al. Quantitative proteomics analysis of triple-negative breast cancers. NPJ Precis Oncol 2025;9(1):117. [CrossRef]
22. Masuda H, Qi Y, Liu S, Hayashi N, Kogawa T, Hortobagyi GN, et al. Reverse phase protein array identification of triple-negative breast cancer subtypes and comparison with mRNA molecular subtypes. Oncotarget 2017;8(41):70481-95. [CrossRef]

Supplementary Table 1. Standardized nomenclature and annotations of the analyzed miRNAs

Pre-miRNA	Mature miRNA	miRBase accession number	Strand specification
hsa-mir-421	hsa-miR-421	MIMAT0002873	5p dominant
hsa-mir-449a	hsa-miR-449a-5p	MIMAT0001541	5p
hsa-mir-378c	hsa-miR-378c	MIMAT0004957	3p/5p reported
hsa-mir-636	hsa-miR-636	MIMAT0003304	Unclear
hsa-mir-618	hsa-miR-618	MIMAT0003280	5p dominant

This table provides complete standardized nomenclature, including miRBase accession numbers and strand dominance, to ensure precise identification and reproducibility.

Supplementary Table 2. Topological centrality metrics of the miRNA–mRNA regulatory network

Node type	Node name	Degree	Betweenness centrality	Closeness centrality
Gene	NQO1	4	0	NA*
Gene	SLC38A1	4	0	NA*
Gene	ALOX15	2	0	NA*
Gene	STEAP3	2	0	NA*
Gene	ACSL6	1	0	NA*
Gene	CP	1	0	NA*
Gene	SLC40A1	1	0	NA*
miRNA	hsa-miR-3662	2	0	0.5
miRNA	hsa-miR-940	2	0	0.5
miRNA	hsa-miR-449a	2	0	0.5
miRNA	hsa-miR-618	1	0	1.0
miRNA	hsa-miR-1270	1	0	1.0
miRNA	hsa-miR-3909	1	0	1.0
miRNA	hsa-miR-7706	1	0	1.0
miRNA	hsa-miR-2110	1	0	1.0
miRNA	hsa-miR-378c	1	0	1.0
miRNA	hsa-miR-636	1	0	1.0
miRNA	hsa-miR-421	1	0	1.0
miRNA	hsa-miR-184	1	0	1.0

This table presents node-level quantitative metrics, including degree, betweenness centrality, and closeness centrality, demonstrating the hierarchical and hub-driven structure of the network. *Closeness centrality for target gene nodes is reported as NA (not applicable) because of the directed, bipartite structure of the network from miRNAs to mRNAs.